Article

Molecular Insights into the Quenching Mechanism of the Triplet Excited State of Rose Bengal through Oxidative and Reductive Organic Compounds

Benjamin Barrios and Daisuke Minakata*

Read Online

ACCESS | Metrics & More | Article Recommendations | SI Supporting Information

ABSTRACT: In oxygenated aquatic environments, the predominant scavenging of the triplet excited state of chromophoric dissolved organic matter (^{3}CDOM*) involves dissolved ground-state oxygen, diverting attention away from the scavenging mechanisms of ^{3}CDOM* mediated through specific organic compounds. Previous studies demonstrated that model ^{3}CDOM* exhibited quantum yields (i.e., 1−56%) in the formation of radical ions, resulting from the competition between physical and chemical quenching through a common exciplex intermediate. Physical quenching was rationalized through the reverse intersystem crossing of the exciplex, followed by back electron transfer, yielding ground-state reactants. Despite this, direct experimental evidence for exciplex involvement has been elusive, owing to detection challenges. Herein, employing density

functional theory (DFT) and time-dependent DFT specifically for excited state surrogate CDOM and organic scavengers, we unveil, for the first time, the underlying mechanisms responsible for the quenching of Rose Bengal through oxidative and reductive scavengers. Our computational findings provide evidence for the involvement of exciplexes during the quenching process of the excited triplet state of Rose Bengal, highlighting the impact of electronic coupling between Rose Bengal and quenchers on the quantum yield for radical ion formation.
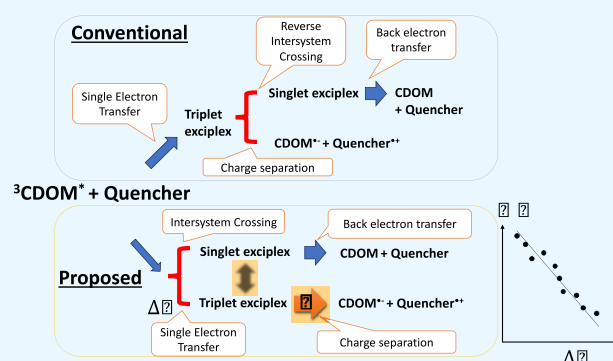
INTRODUCTION

In environmental waters, dissolved organic matter (DOM) is a complex mixture of organic carbons resulting from the dissolution of environmental products and anthropogenic contaminants.[1,2] DOM affects the abiotic and microbial fate and transport of contaminants[3] and formation of disinfection byproducts during drinking water treatment.[4] Chromophoric DOM (CDOM) absorbs sunlight and is involved in the photochemical fate of the contaminants.

Photochemically produced reactive intermediates (PPRIs), such as the triplet excited state of CDOM (^{3}CDOM*), singlet oxygen, hydroxyl radicals, and hydrogen peroxide, play important roles in determining the abiotic fate of organic and inorganic compounds in surface waters exposed to sunlight irradiation.[5−8] Among the PPRIs, ^{3}CDOM* is the major contributor to the photochemical fate of organic compounds, undergoing single electron transfer (SET) or proton coupled ET reactions that generate the radical anion of CDOM (CDOM$^{•−}$) and the radical cation of the organic compound (R$^{•+}$).[5,9−11] CDOM$^{•−}$ reacts with dissolved oxygen in water to reproduce CDOM, while R$^{•+}$ irreversibly decomposes to R$^{•}$ + H$^+$ via deprotonation.[12,13]

Despite extensive studies on the kinetics of ^{3}CDOM* quenching using a surrogate and standard CDOM,[5,14,15]

knowledge gaps persist regarding the quenching mechanism, primarily owing to the major scavenging of ^{3}CDOM* through dissolved oxygen, preventing detailed investigations. The quenching process of ^{3}CDOM* via a quencher (Q) involves the formation of an encounter complex ($[^3$CDOM* + Q]$) (Scheme 1).[16−19] This encounter complex undergoes SET to generate the triplet state of an exciplex ($^3[$CDOM$^{•−}$···Q$^{•+}]$*) that can either dissociate to form the free radical ions of CDOM$^{•−}$ and Q$^{•+}$ or regenerate ground-state CDOM and Q via back electron transfer (bET). Notably, the ground-state CDOM and Q exist in singlet multiplicity, leading to the reverse intersystem crossing (rISC) of the exciplex and the formation of the singlet state of an exciplex ($^1[$CDOM$^{•−}$···Q$^{•+}]$*). Although previous studies successfully explained the kinetics of the encounter complex mechanism using Marcus or Rehm−Weller equations for the outer-sphere SET,[5,14,20]

Scheme 1. Postulated Mechanism for Chemical and Physical Quenching of ^{3}CDOM* by a Quencher, Q

$$^3\text{CDOM}^* + \text{Q} \rightleftharpoons [^3\text{CDOM}^* + \text{Q}] \xrightarrow{\text{SET}} {}^3[\text{CDOM}^{\bullet-} \cdots \text{Q}^{\bullet+}]^* \xrightarrow[\text{fast}]{} \text{CDOM}^{\bullet-} + \text{Q}^{\bullet+}$$

Encounter complex   Exciplex   free radical ions

ISC ↕ rISC

$$^1[\text{CDOM}^{\bullet-} \cdots \text{Q}^{\bullet+}]^*$$

↓ bET

$$\text{CDOM} + \text{Q}$$

experimentally observed smaller quantum yields (e.g., 0.01 to 0.56)[11,16,21−24] for the formation of the free radical ions of CDOM$^{\bullet-}$ and Q$^{\bullet+}$ could not account for the regeneration of ground-state CDOM and Q. The absence of experimental evidence is attributed to the difficulties in identifying such an exciplex of surrogate CDOM in the aqueous-phase, characterized by a short lifetime in the range from 10^{-9}–10^{-12} s[25,26] owing to rapid electronic transitions. Consequently, alternative approaches that connect the experimentally observed stable products with the electronic structure of the intermediate exciplexes must be undertaken. Quantum mechanics (QM)-based computations can provide the energies of the different excited states of encounter complexes and their individual components.[27,28]

Herein, we employ QM-based density functional theory (DFT) and time-dependent DFT (TD-DFT) calculations to provide computational evidence supporting the involvement of exciplexes in the regeneration of ground-state CDOM and Q via rISC and bET using Rose Bengal (RB^{2-}) as a surrogate CDOM, while structurally diverse organic compounds function as an oxidative or a reductive Q in the absence of dissolved oxygen. Based on strong correlations between experimentally obtained quantum yields for the formation of free radical ions of RB^{2-} and Q, as reported in the literature, and the molecular properties of the exciplexes, we propose a new reaction pathway for the quenching of the triplet excited state of RB^{2-} (^{3}RB^{2-}*). We underpin the overlooked role of electronic coupling in SET reactions within the photochemically excited CDOM of aqueous phase environmental samples.

MATERIALS AND METHODS

Data Collection. We compiled 12 experimentally obtained quantum yields (Φ) pertaining to the quenching of the triplet excited state of RB^{2-} for the formation of free radical ions in the deoxygenated aqueous solution at neutral pH.[16] Table S1 in the SI summarizes the chemical structure of RB^{2-} and the 12 Qs.

QM-Based DFT and TD-DFT Calculations. Owing to the substantial size of some complexes containing more than 60 atoms with heavy elements, conducting geometry optimization followed by frequency calculations and subsequent TD-DFT calculations becomes computationally prohibitive. To strike a balance between computational cost and accuracy, 6-31+G(d) basis set was selected owing to the previous prediction of electronic transitions of organic molecules[29,30] and our benchmark calculations and the validation with the experimental values (Text S2 in the SI). Geometry optimization for the complexes and their individual compounds was conducted using the M06-2X[31]/6-31 + G(d) level of theory with the universal solvation model based on the electron density of the

solute.[32] For iodine atoms of RB^{2-}, the Los Alamos National Lab (LANL2DZ) pseudopotential with frozen core electrons was used.[33] The selection of the M06-2X exchange-correlation functional was driven by its accuracy in estimating the geometries of organic compounds and intermolecular interactions.[34] We also conducted geometry optimizations of the complexes employing two additional hybrid exchange-correlation functionals, BMK[35] and ω-B97X-D,[36] which incorporate dispersion corrections for noncovalent corrections. Table S2 in the SI compares energies at the first singlet and triplet excited states of RB^{2-} obtained at different DFT functionals and basis sets to experimental values. Text S1 in the SI provides a detailed discussion of the comparison.

For the geometry optimization of a complex and an exciplex, we optimized the minimum-energy molecular geometries of RB^{2-} and the 12 Qs at the ground state. To determine the molecular structure of a complex involving RB^{2-} and each Q, the highest occupied molecular orbital (HOMO) and lowest unoccupied molecular orbital (LUMO) were calculated first (Figures S1 and S2 in the SI). We then placed each Q in a cofacial orientation to the xanthene group of RB^{2-} to maximize the overlap between the HOMO and LUMO, employing a conformer search procedure previously developed in the literature.[37−40] Text S2 in the SI provides a detailed geometry optimization procedure. Figure S3 in the SI shows the examples of constructive interference of RB^{2-} and oxidative or reductive Q. All the computations were performed using *Gaussian 16* Revision C.01[41] at Michigan Tech HPC cluster "Superior" and homemade workstations.

For simulating the unimolecular SET reaction of the complex, we used the Marcus equation (eq 1), as shown below:[27,42]

$$k_{\text{ET}} = \frac{2\pi}{h}|H|^2 \sqrt{\frac{1}{4\pi k_{\text{B}}T\lambda}} e^{-(\lambda + \Delta E_{\text{ET}})/(4\lambda k_{\text{B}}T)} \tag{1}$$

where k_{ET} is the unimolecular reaction rate constant, H is the electronic tunneling matrix element between an electron donor and an acceptor,[43] λ is the reorganization energy for the SET reaction, h is the Planck constant, T is the absolute temperature, and k_{B} is the Boltzmann constant. ΔE_{ET} is the energy difference between the triplet excited state of a complex (i.e., exciplex) and the encounter complex [^{3}RB^{2-}* + Q]. The H value exhibits an exponential dependency on the separation distance, r, between the RB^{2-} and Q, as shown in eq 2; thus, the k_{ET} value maintains an exponential relation with the r value:[44−46]

$$|H|^2 \propto e^{[-\beta(r-r_0)]} \tag{2}$$

where β is the decay parameter of a contact distance to the H value, and r_0 is the contact distance between RB^{2-} and Q. Here, using the coordinates of an optimized complex, we determined the r-value, defined as the distance between the center of the RB^{2-} benzene, yielding the delocalized negative charge (i.e., the site at HOMO), and the center of the ring on oxidative Qs (i.e., the site at LUMO) such as methyl viologen (MV), anthraquinone-2-sulfonate (AQS), duroquinone (DQ), dimethylbenzoquinone (DMBQ), 4-nitroimidazole (4NI), 2-nitroimidazole (2NI), and benzoquinone (BQ). For reductive Qs such as tryptophan (TRP), cysteine (CYS), tyrosine (TYR), hydroquinone (HQ), and ascorbate (ASC), we used the distance between the heteroatom of Q (i.e., the site at HOMO) and the center of the pyran ring in RB^{2-} (i.e., the site at LUMO). Figure 1 shows schematics illustrating the definition of r using examples of quinone and hydroxylated benzene base structures for oxidative and reductive Qs, respectively.
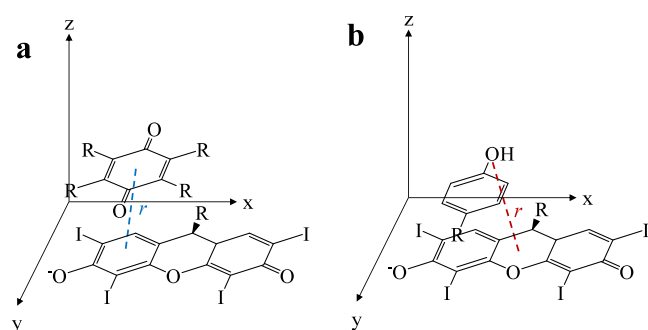
Figure 1. Definition of the separation distance, r, for a complex between RB^{2-} and Q (quinone, a; hydroxylated benzene, b).

The rate of ISC or rISC, where the rate constant is defined as k_{ISC}, is governed by the spin−orbit coupling (SOC), represented as the term $\langle S|\hat{H}_{SOC}|T\rangle$, and the energy difference between triplet and singlet exciplex, ΔE_{ISC}, according to eq 3:[47]

$$k_{ISC} \propto |\langle S|\hat{H}_{SOC}|T\rangle|^2 \exp(-\Delta E_{ISC}^2) \qquad (3)$$

■ RESULTS AND DISCUSSION

Molecular Structures of the Encounter Complex. The optimized molecular structure of RB^{2-} exhibits HOMO localized on the aromatic rings of the xanthene moiety (Figure S1 in the SI), showcasing delocalization of the negative charges (Figure S4 in the SI), consistent with previous observations.[48] The LUMO orbital is located on the central pyran ring of RB^{2-} (Figure S1 in the SI). Figure 2 represents the HOMO and LUMO of the complex of RB^{2-} and oxidative and reductive Qs, illustrated by using benzoquinone and tyrosine as examples, respectively. Additionally, Figure S5 in the SI shows the HOMO and LUMO of all other complexes with oxidative and reductive Qs. For oxidative Qs, the optimized structure of the complex featuring RB^{2-} and benzoquinone shows a cofacial $\pi-\pi$ stacking arrangement between the HOMO site of RB^{2-} and the LUMO site of benzoquinone (Figure 2a). For reductive Qs, the LUMO of RB^{2-} aligns cofacially with the HOMO of tyrosine (Figure 2b). The analysis of the molecular structures of the encounter complexes indicates the importance of the electronic structures of both RB^{2-} and oxidative or reductive Qs.
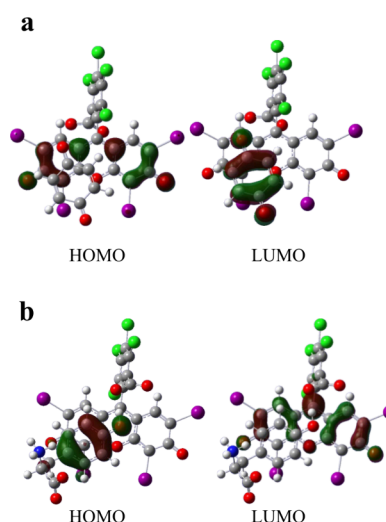
Figure 2. HOMO and LUMO structures of complexes of both RB^{2-} and oxidative (i.e., benzoquinone) (a) or reductive (i.e., tyrosine) (b) Qs.

To investigate the physical distance between RB^{2-} and Q within an encounter complex, Figure 3 plots the r values
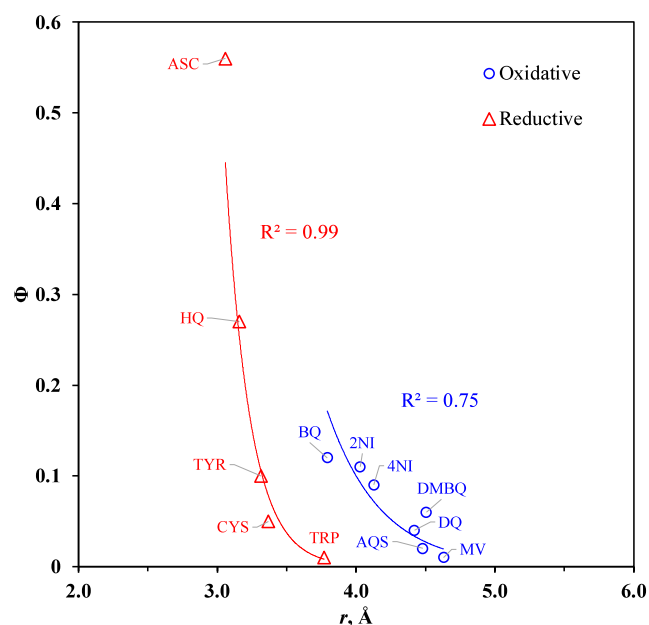
Figure 3. Correlations between Φ[16] and r for oxidative and reductive Qs. Lines are approximated based on the exponential function.

obtained through M06-2X and Φ values, while Table 1 includes each r value along with other molecular orbital energies of the exciplex and the ΔE_{ET} and ΔE_{ISC} values alongside experimental Φ values. The exponential correlation observed between r and Φ values for oxidative and reductive Qs confirms the inverse relation with the electron transfer rate, as per eq 2, indicating the impact of the physical distance between RB^{2-} and Q of the complex on the yield of radical ions. Geometry optimizations of the complex were also conducted using other hybrid exchange-correlation functions of BMK and ω-B97X-D, which include dispersion corrections for noncovalent interactions, confirming the same trend as those obtained by M06-2X (Figure S6 in the SI).

Table 1. Interaction Distance between RB^{2-} and Q, Exciplex Energies of Triplet and Singlet States, Electron Transfer, and ISC Energies for Oxidative and Reductive Qs Calculated at the Level of M06-2X, and Experimentally Determined Φ Values

Q	r, Å	energy of triplet exciplex, kcal/mol	energy of singlet exciplex, kcal/mol	ΔE_{ET}, kcal/mol	ΔE_{ISC}, kcal/mol	Φ[16]
methyl viologen (MV)	4.6	51.0	51.3	13.3	0.2	0.01
anthraquinone-2-sulfonate (AQS)	4.5	44.5	44.7	6.8	0.2	0.02
duroquinone (DQ)	4.4	44.7	45.3	7.0	0.6	0.04
dimethyl benzoquinone (DMBQ)	4.5	40.3	40.8	2.6	0.5	0.06
4-nitroimidazole (4NI)	4.1	41.9	42.4	4.2	0.5	0.09
2-nitroimidazole (2NI)	4.0	34.0	34.4	−3.7	0.4	0.11
benzoquinone (BQ)	3.8	36.0	37.2	−1.7	1.2	0.12
tryptophan (TRP)	3.8	54.6	55.0	16.9	0.4	0.01
cysteine (CYS)	3.4	79.1	79.2	41.4	0.1	0.05
tyrosine (TYR)	3.3	67.1	69.0	29.4	2.0	0.10
hydroquinone (HQ)	3.2	59.2	61.1	21.5	2.0	0.27
ascorbate (ASC)	3.1	43.4	44.3	5.7	0.9	0.56
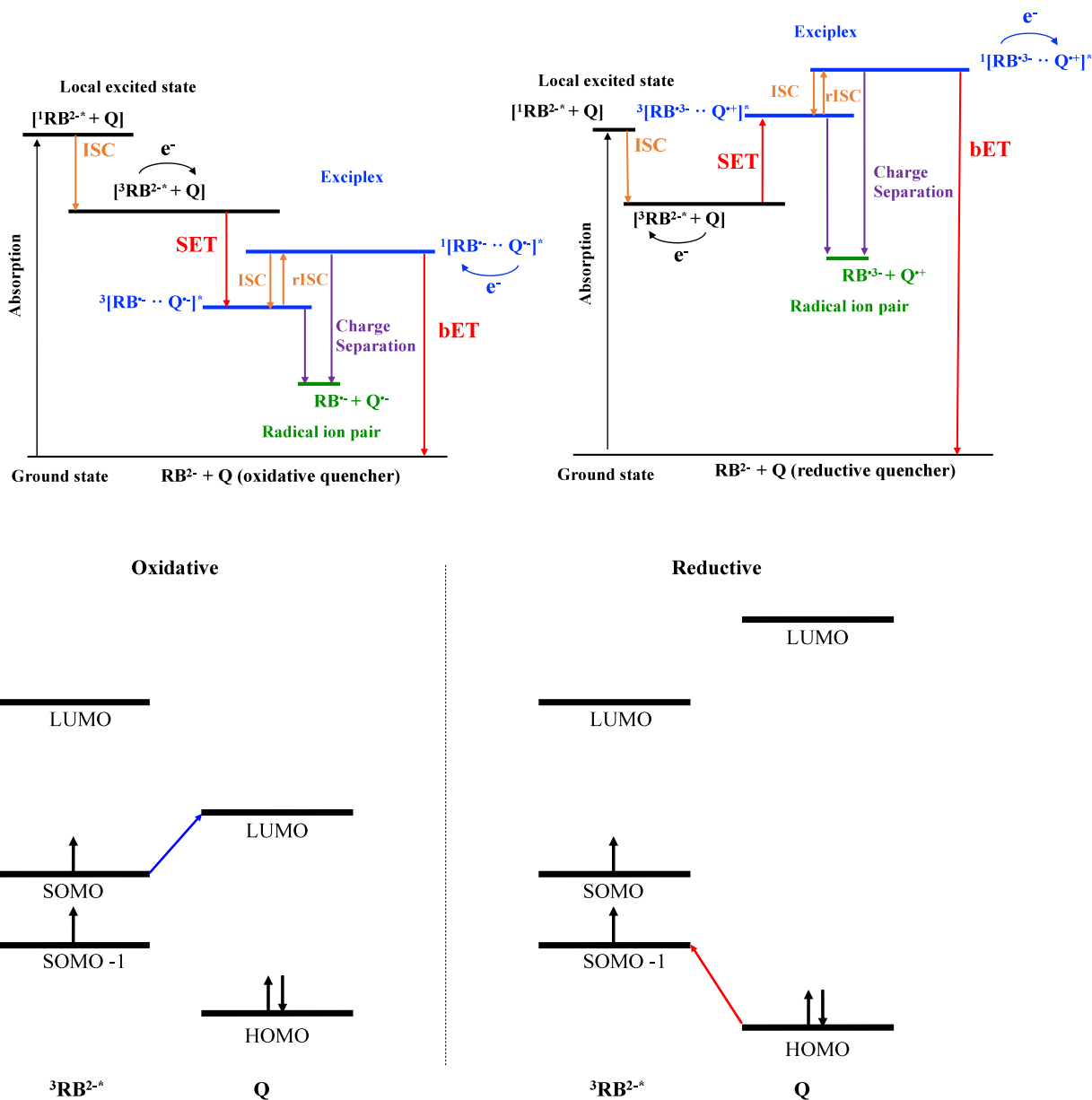
Figure 4. Jablonski diagrams (top) of RB^{2-} with oxidative Q (left) and reductive Q (right) and schematic frontier molecular orbital diagram (bottom) for oxidative (left) and reductive (right) quenching.
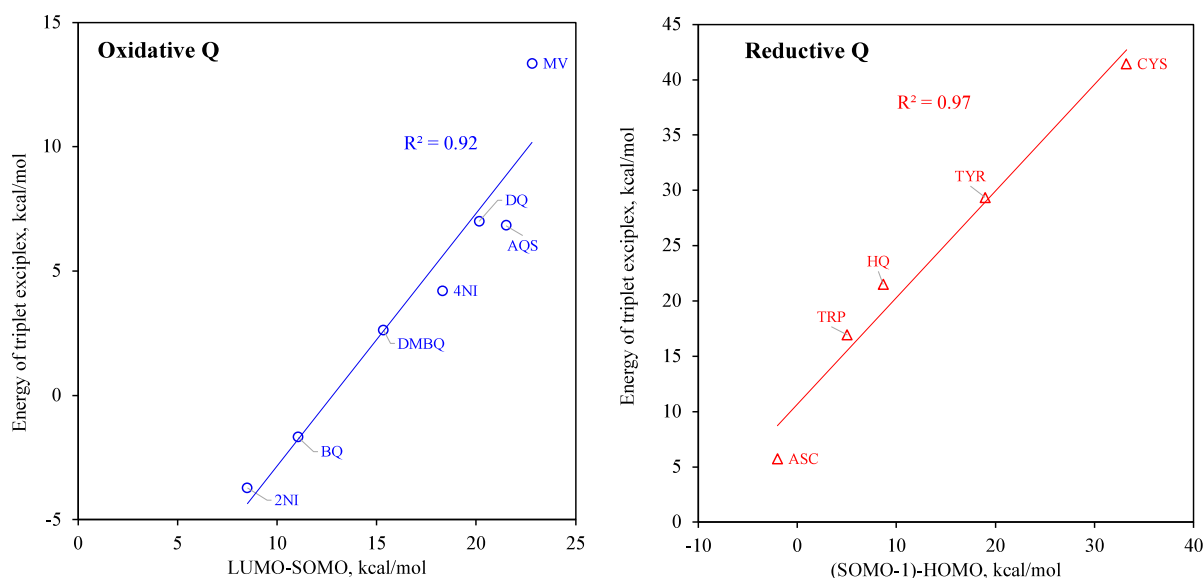
Figure 5. Plots of LUMO-SOMO and (SOMO-1)-HOMO vs energy of the triplet exciplex for oxidative (left) and reductive (right) Qs. Energy gaps and triplet exciplex energy values obtained at the PBE0/6-31+G(d)+LANL2DZ level of theory with the SMD solvation model.

Electronic Structures of the Encounter Complex and Exciplex. Utilizing the energies at the excited states of each RB^{2-}, Q, and complex, general Jablonski diagrams were constructed for oxidative and reductive Qs separately (Figure 4). Tables S3−S27 in the SI show energy values for all Qs. Once the precursor complex of the triplet excited state of RB^{2-} (i.e., $^3RB^{2-}*$) and Q is formed, a SET occurs inside the complex, forming a triplet state of the exciplex. Subsequently, the exciplex undergoes reversible rISC, resulting in a singlet state of the exciplex. This singlet state further undergoes bET, regenerating RB^{2-} and Q. Charge separation in both exciplexes generates a radical ion pair of RB^{2-} and Q. A detailed discussion of the electronic structures of the complex and exciplex is as follows.

In oxidative quenching, an electron transitions from the singly occupied molecular orbital (SOMO) of $^3RB^{2-}*$ to the LUMO of Q, whereas in reductive quenching, an electron flows from the HOMO of Q to the SOMO of $^3RB^{2-}*$ (Figure 4). Thus, the LUMO−SOMO and SOMO−HOMO energy gaps strongly correlate with the corresponding energy of triplet exciplex for oxidative and reductive quenching, respectively (Figure 5). Because the HOMO−LUMO energies depend on the DFT functionals,[49,50] other functionals that included range-separated corrections and different degreees of Hartree−Fock exchange functionals (i.e., ω-B97X-D and BMK) were used to calculate the HOMO−LUMO energies and confirmed the consistent correlations with those obtained by PBE0 (Figures S7 and S8 in the SI). Notably, the correlations are evident for the first singlet excited state (S1), first triplet excited state (T1), and redox potentials of Q with the energy of the triplet exciplex in reductive quenching but not in oxidative quenching (Figures S9 and S10 in the SI). Evidently, the redox potentials of Q are intrinsically related to the HOMO of a molecule, and the HOMO is not involved in the SET process for oxidative Qs.

Rate-Determining Step for the Formation of Radical Pair and Reaction Mechanisms. The previously postulated reaction mechanism in Scheme 1 and eq 3 indicates that if the rate of rISC (k_{rISC}) is the rate-limiting factor for bET, then Φ should exhibit a linear correlation with the ΔE_{ISC} values

because of the limited conversion of electrons to its triplet exciplex. However, the plot of the ΔE_{ISC} values of all Qs against a natural logarithm of Φ does not exhibit any correlations ($r^2 < 0.4$ for all cases), as observed with three DFT methods (Figure S11 in the SI). We then investigated the correlation with the ΔE_{ET} values of all of the Qs. Figure 6
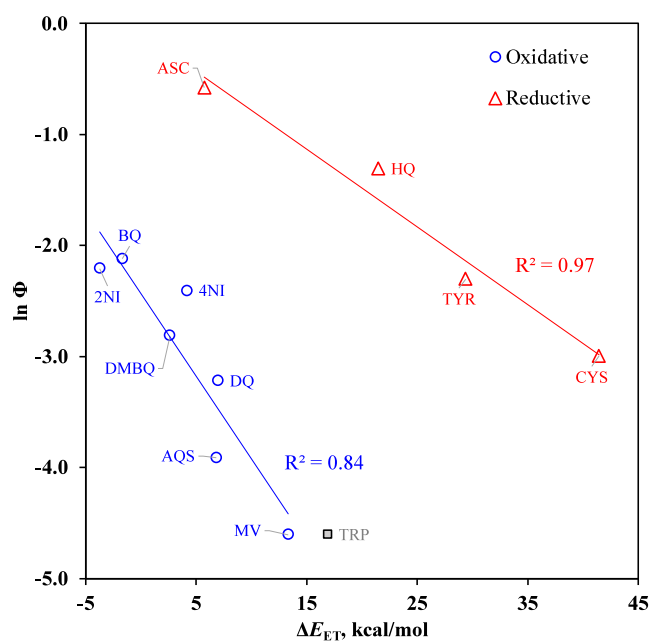
**Figure 6.** ln Φ^{16} vs ΔE_{ET} for oxidative and reductive Qs.

exhibits a strong linear correlation between ln Φ and ΔE_{ET} values, except for a data point for TRP as a reductive Q. Further verification with two other DFT methods confirmed the overall trend (Figures S12 in the SI), highlighting the exception of TRP. The abnormally larger r values of TRP appear to cause the inconsistent trend observed in Figure 6.

Previously, Φ values were determined based on the degree of bET proceeding through the rISC from triplet to singlet

exciplex.[16,17] However, our theoretical calculations for the Φ dependence on r and ΔE_{ET} collectively demonstrate that the SET step exerts an enhanced influence on the measured values of Φ. Thus, we propose that during the formation of an encounter complex between $^3RB^{2-}$* and Q, ISC to the singlet exciplex competes with SET to the triplet exciplex (Scheme 2).

Scheme 2. Comparison of the Conventional and Our Proposed Model for $^3RB^{2-}$* Quenching through an Electron Donor Q

Conventional model:
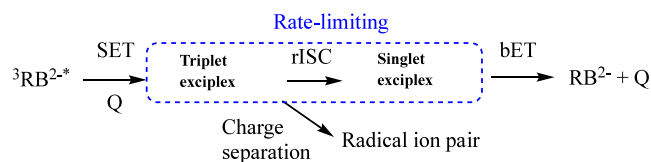
Proposed model:
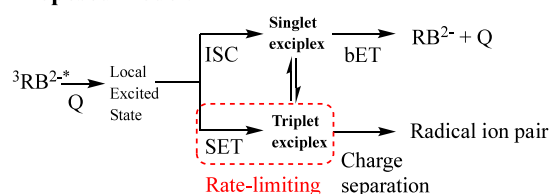
Moreover, we propose that the rate of ISC to the singlet exciplex is notably faster than that of SET, which explains why only exciplexes with small values of r and ΔE_{ET} display relatively large values of Φ for the formation of the radical ion pair. When the coupling between $^3RB^{2-}$* and Q is low (resulting in large separation distance r) and ΔE_{ET} is large, ISC to a singlet exciplex followed by bET becomes dominant to yield ground state RB^{2-} and Q, leading to less formation of radical ion pair and consequently low values of Φ. The fast ISC from $^3RB^{2-}$* to the singlet exciplex can be attributed to the amplification of the SOC induced by iodine atoms in the structure of RB^{2-}, in combination with the small energy difference between $^3RB^{2-}$* and the singlet exciplex. Previous studies have demonstrated that the presence of heavy atoms in the structure of either the photosensitizer or the Q greatly decreases Φ for radical ion formation.[19,51]

CONCLUSIONS

It is estimated that under normal air-saturated environmental surface water conditions, relaxation of ^3CDOM* via dissolved ground state triplet oxygen, $^3O_2$, ($k_{O_2} \times [O_2]$, where k_{O_2} is the second order rate constant of $^3O_2$ with ^3CDOM* and $[O_2]$ is approximately 8−9 mg/L) is faster than the $^3O_2$-independent relaxation (k_D is the first order relaxation rate of ^3CDOM*) by an order of magnitude.[5] This dominant $^3O_2$-dependent relaxation of ^3CDOM* generally hinders the minor scavenging of ^3CDOM* by organic compounds. The results of this study suggest the importance of the geometrical conformation of the encounter complex formed by $^3RB^{2-}$* and a biologically relevant quencher in SET reactions. This stands in contrast to the commonly assumed outer-sphere mechanism, where quenching occurs through an electron transfer without necessitating a specific orientation. It has long been known that SET reactions lack a well-defined stationary structure on the potential energy surface representing the reaction extent.[52] Herein, we offer an alternative concept, demonstrating that

SET occurs within complexes where molecules are arranged in a specific orientation, facilitating orbital overlap, and creating a pathway for electron transfer. Understanding the geometrical and electronic parameters that control the efficiency of triplet quenching of surrogate CDOM provides mechanistic insight into the reactivity of a complex mixture of CDOM that is present in natural aquatic environments. Holistic understanding of triplet quenching of a diverse surrogate CDOM will enhance our ability to make accurate predictions regarding the fate of organic contaminants in natural waters.

Further experimental investigations employing different model CDOM are essential to fully comprehend the role of exciplex conformation and charge transfer states on Φ values. Systematic studies involving the introduction of a steric hindrance to model CDOM while keeping the molecular and electronic structure of the Q constant would provide additional insights into the dependence of Φ on the separation distance between CDOM and Q. We envision that experiments in which one organic quencher is used as a reference by incrementally accommodating a variety of functional groups will allow one to systematically investigate the steric effect of functional groups. Model CDOM compounds with less pronounced ISC than in RB^{2-} are necessary to validate the present results without competing ISC/SET. For example, the use of quinones as model CDOM is a potential way to exploring the SET mechanism because of their greater oxidizing abilities in the excited triplet state than other surrogate CDOM. Further, lack of heavy elements could accelerate ISC.

■ ASSOCIATED CONTENT

ⓢ Supporting Information

The Supporting Information is available free of charge at https://pubs.acs.org/doi/10.1021/acsomega.4c04759.

> Quantum-mechanical calculations and geometry optimization of a complex and an exciplex, twenty-eight tables, including the chemical structure of rose bengal and 12 quenchers, energies of the first singlet and triplet excited states of rose bengal and 12 quenchers, and ten figures of HOMO and LUMO, resonance structures of rose bengal and complex, correlation of quantum yield of quenching and r values, correlation of energies of ISC and electron transfer, and xyz Cartesian coordinates of optimized molecules and complexes (PDF)

■ AUTHOR INFORMATION

Corresponding Author

Daisuke Minakata − *Department of Civil, Environmental and Geospatial Engineering, Michigan Technological University, Houghton, Michigan 49931, United States;* ⓞ orcid.org/0000-0003-3055-3880; Phone: +1-906-487-1830; Email: dminakat@mtu.edu; Fax: +1-906-487-2943

Author

Benjamin Barrios − *Department of Civil, Environmental and Geospatial Engineering, Michigan Technological University, Houghton, Michigan 49931, United States*

Complete contact information is available at:
https://pubs.acs.org/10.1021/acsomega.4c04759

Notes

The authors declare no competing financial interest.

REFERENCES

(1) Buffam, I.; Turner, M. G.; Desai, A. R.; Hanson, P. C.; Rusak, J. A.; Lottig, N. R.; Stanley, E. H.; Carpenter, S. R. Integrating aquatic and terrestrial components to construct a complete carbon budget for a north temperate lake district. *Glob. Change Biol.* **2011**, *17* (2), 1193−1211.

(2) Tranvik, L. J.; Downing, J. A.; Cotner, J. B.; Loiselle, S. A.; Striegl, R. G.; Ballatore, T. J.; Dillon, P.; Finlay, K.; Fortino, K.; Knoll, L. B.; et al. Lakes and reservoirs as regulators of carbon cycling and climate. *Limnol. Oceanogr.* **2009**, *54* (6part2), 2298−2314.

(3) Aiken, G. R.; Hsu-Kim, H.; Ryan, J. N. Influence of Dissolved Organic Matter on the Environmental Fate of Metals, Nanoparticles, and Colloids. *Environ. Sci. Technol.* **2011**, *45* (8), 3196−3201.

(4) Rook, J. J. Chlorination reactions of fulvic acids in natural waters. *Environ. Sci. Technol.* **1977**, *11* (5), 478−482.

(5) Schmitt, M.; Erickson, P. R.; McNeill, K. Triplet-State Dissolved Organic Matter Quantum Yields and Lifetimes from Direct Observation of Aromatic Amine Oxidation. *Environ. Sci. Technol.* **2017**, *51* (22), 13151−13160.

(6) Zepp, R. G.; Wolfe, N. L.; Baughman, G. L.; Hollis, R. C. Singlet oxygen in natural waters. *Nature* **1977**, *267* (5610), 421−423.

(7) Boreen, A. L.; Edhlund, B. L.; Cotner, J. B.; McNeill, K. Indirect Photodegradation of Dissolved Free Amino Acids: The Contribution of Singlet Oxygen and the Differential Reactivity of DOM from Various Sources. *Environ. Sci. Technol.* **2008**, *42* (15), 5492−5498.

(8) Yang, Y.; Sun, P.; Padhye, L. P.; Zhang, R. Photo-ammonification in surface water samples: Mechanism and influencing factors. *Sci. Total Environ.* **2021**, *759*, 143547.

(9) McNeill, K.; Canonica, S. Triplet state dissolved organic matter in aquatic photochemistry: reaction mechanisms, substrate scope, and photophysical properties. *Environ. Sci. Process. Impacts* **2016**, *18* (11), 1381−1399.

(10) Rosario-Ortiz, F. L.; Canonica, S. Probe Compounds to Assess the Photochemical Activity of Dissolved Organic Matter. *Environ. Sci. Technol.* **2016**, *50* (23), 12532−12547.

(11) Kong, Q.; Pan, Y.; Lei, X.; Zhou, Y.; Lei, Y.; Peng, J.; Zhang, X.; Yin, R.; Shang, C.; Yang, X. Reducing properties of triplet state organic matter (3DOM*) probed via the transformation from chlorine dioxide to chlorite. *Water Res.* **2022**, *225*, 119120.

(12) Nicholas, A. M. d. P.; Arnold, D. R. Thermochemical parameters for organic radicals and radical ions. Part 1. The estimation of the pKa of radical cations based on thermochemical calculations. *Can. J. Chem.* **1982**, *60* (17), 2165−2179.

(13) Jonsson, M.; Wayner, D. D. M.; Lusztyk, J. Redox and Acidity Properties of Alkyl- and Arylamine Radical Cations and the Corresponding Aminyl Radicals. *J. Phys. Chem.* **1996**, *100* (44), 17539−17543.

(14) Erickson, P. R.; Walpen, N.; Guerard, J. J.; Eustis, S. N.; Arey, J. S.; McNeill, K. Controlling Factors in the Rates of Oxidation of Anilines and Phenols by Triplet Methylene Blue in Aqueous Solution. *J. Phys. Chem. A* **2015**, *119* (13), 3233−3243.

(15) Canonica, S.; Hellrung, B.; Wirz, J. Oxidation of Phenols by Triplet Aromatic Ketones in Aqueous Solution. *J. Phys. Chem. A* **2000**, *104* (6), 1226−1232.

(16) Lambert, C. R.; Kochevar, I. E. Electron Transfer Quenching of the Rose Bengal Triplet State. *Photochem. Photobiol.* **1997**, *66* (1), 15−25.

(17) Gould, I. R.; Ege, D.; Moser, J. E.; Farid, S. Efficiencies of photoinduced electron-transfer reactions: role of the Marcus inverted region in return electron transfer within geminate radical-ion pairs. *J. Am. Chem. Soc.* **1990**, *112* (11), 4290−4301.

(18) Gould, I. R.; Young, R. H.; Moody, R. E.; Farid, S. Contact and solvent-separated geminate radical ion pairs in electron-transfer photochemistry. *J. Phys. Chem.* **1991**, *95* (5), 2068−2080.

(19) Steiner, U.; Winter, G.; Kramer, H. E. A. Investigation of physical triplet quenching by electron donors. *J. Phys. Chem.* **1977**, *81* (11), 1104−1110.

(20) Rehm, D.; Weller, A. Kinetics of Fluorescence Quenching by Electron and H-Atom Transfer. *Isr. J. Chem.* **1970**, *8* (2), 259−271.

(21) Rizzuto, F.; Spikes, J. D. The Eosin-Sensitized Photooxidation of Substituted Phenylalanines and Tyrosines*. *Photochem. Photobiol.* **1977**, *25* (5), 465−476.

(22) Ludvíková, L.; Štacko, P.; Sperry, J.; Klán, P. Photosensitized Cross-Linking of Tryptophan and Tyrosine Derivatives by Rose Bengal in Aqueous Solutions. *J. Org. Chem.* **2018**, *83* (18), 10835−10844.

(23) Sarna, T.; Zając, J.; Bowman, M. K.; Truscott, T. G. Photoinduced electron transfer reactions of rose bengal and selected electron donors. *J. Photochem. Photobiol., A* **1991**, *60* (3), 295−310.

(24) Miller, B. L.; Williams, T. D.; Schöneich, C. Mechanism of Sulfoxide Formation through Reaction of Sulfur Radical Cation Complexes with Superoxide or Hydroxide Ion in Oxygenated Aqueous Solution. *J. Am. Chem. Soc.* **1996**, *118* (45), 11014−11025.

(25) Potocny, A. M.; Phelan, B. T.; Sprague-Klein, E. A.; Mara, M. W.; Tiede, D. M.; Chen, L. X.; Mulfort, K. L. Harnessing Intermolecular Interactions to Promote Long-Lived Photoinduced Charge Separation from Copper Phenanthroline Chromophores. *Inorg. Chem.* **2022**, *61* (48), 19119−19133.

(26) Gould, I. R.; Young, R. H.; Mueller, L. J.; Albrecht, A. C.; Farid, S. Electronic Structures of Exciplexes and Excited Charge-Transfer Complexes. *J. Am. Chem. Soc.* **1994**, *116* (18), 8188−8199.

(27) Veldkamp, B. S.; Liu, X.; Wasielewski, M. R.; Subotnik, J. E.; Ratner, M. A. Molecular Excited States: Accurate Calculation of Relative Energies and Electronic Coupling Between Charge Transfer and Non-Charge Transfer States. *J. Phys. Chem. A* **2015**, *119* (2), 253−262.

(28) Schleper, A. L.; Goushi, K.; Bannwarth, C.; Haehnle, B.; Welscher, P. J.; Adachi, C.; Kuehne, A. J. C. Hot exciplexes in U-shaped TADF molecules with emission from locally excited states. *Nat. Commun.* **2021**, *12* (1), 6179.

(29) Shizu, K.; Kaji, H. Theoretical Determination of Rate Constants from Excited States: Application to Benzophenone. *J. Phys. Chem. A* **2021**, *125* (40), 9000−9010.

(30) Shizu, K.; Ren, Y.; Kaji, H. Promoting Reverse Intersystem Crossing in Thermally Activated Delayed Fluorescence via the Heavy-Atom Effect. *J. Phys. Chem. A* **2023**, *127* (2), 439−449.

(31) Zhao, Y.; Truhlar, D. G. The M06 suite of density functionals for main group thermochemistry, thermochemical kinetics, non-covalent interactions, excited states, and transition elements: two new functionals and systematic testing of four M06-class functionals and 12 other functionals. *Theor. Chem. Acc.* **2008**, *120* (1), 215−241.

(32) Marenich, A. V.; Cramer, C. J.; Truhlar, D. G. Universal Solvation Model Based on Solute Electron Density and on a Continuum Model of the Solvent Defined by the Bulk Dielectric Constant and Atomic Surface Tensions. *J. Phys. Chem. B* **2009**, *113* (18), 6378−6396.

(33) Hay, P. J.; Wadt, W. R. Ab initio effective core potentials for molecular calculations. Potentials for K to Au including the outermost core orbitals. *J. Phys. Chem.* **1985**, *82* (1), 299−310.

(34) Zhao, Y.; Truhlar, D. G. Density Functionals with Broad Applicability in Chemistry. *Acc. Chem. Res.* **2008**, *41* (2), 157−167.

(35) Boese, A. D.; Martin, J. M. L. Development of density functionals for thermochemical kinetics. *J. Chem. Phys.* **2004**, *121* (8), 3405−3416.

(36) Chai, J.-D.; Head-Gordon, M. Long-range corrected hybrid density functionals with damped atom-atom dispersion corrections. *Phys. Chem. Chem. Phys.* **2008**, *10* (44), 6615−6620.

(37) Lindquist, R. J.; Lefler, K. M.; Brown, K. E.; Dyar, S. M.; Margulies, E. A.; Young, R. M.; Wasielewski, M. R. Energy Flow Dynamics within Cofacial and Slip-Stacked Perylene-3,4-dicarboximide Dimer Models of π-Aggregates. *J. Am. Chem. Soc.* **2014**, *136* (42), 14912−14923.

(38) Nagami, T.; Ito, S.; Kubo, T.; Nakano, M. Intermolecular Packing Effects on Singlet Fission in Oligorylene Dimers. *ACS Omega* **2017**, *2* (8), 5095−5103.

(39) Polizzi, N. F.; Migliore, A.; Therien, M. J.; Beratan, D. N. Defusing redox bombs? *Proc. Natl. Acad. Sci. U. S. A.* **2015**, *112* (35), 10821−10822.

(40) Rosokha, S. V.; Newton, M. D.; Head-Gordon, M.; Kochi, J. K. Mulliken-Hush elucidation of the encounter (precursor) complex in intermolecular electron transfer via self-exchange of tetracyanoethylene anion-radical. *Chem. Phys.* **2006**, *324* (1), 117−128.

(41) *Gaussian 16*, Rev. C.01; Gaussian: Wallingford, CT, 2016.

(42) Marcus, R. A. Chemical and Electrochemical Electron-Transfer Theory. *Annu. Rev. Phys. Chem.* **1964**, *15* (1), 155−196.

(43) Beratan, D. N.; Betts, J. N.; Onuchic, J. N. Protein Electron Transfer Rates Set by the Bridging Secondary and Tertiary Structure. *Science* **1991**, *252* (5010), 1285−1288.

(44) Risser, S. M.; Beratan, D. N.; Meade, T. J. Electron transfer in DNA: predictions of exponential growth and decay of coupling with donor-acceptor distance. *J. Am. Chem. Soc.* **1993**, *115* (6), 2508−2510.

(45) Gray, H. B.; Winkler, J. R. Long-range electron transfer. *Proc. Natl. Acad. Sci. U. S. A.* **2005**, *102* (10), 3534−3539.

(46) Gray, H. B.; Winkler, J. R. Hole hopping through tyrosine/tryptophan chains protects proteins from oxidative damage. *Proc. Natl. Acad. Sci. U. S. A.* **2015**, *112* (35), 10920−10925.

(47) Ma, H.; Peng, Q.; An, Z.; Huang, W.; Shuai, Z. Efficient and Long-Lived Room-Temperature Organic Phosphorescence: Theoretical Descriptors for Molecular Designs. *J. Am. Chem. Soc.* **2019**, *141* (2), 1010−1015.

(48) Buck, S. T. G.; Bettanin, F.; Orestes, E.; Homem-de-Mello, P.; Imasato, H.; Viana, R. B.; Perussi, J. R.; da Silva, A. B. F. Photodynamic Efficiency of Xanthene Dyes and Their Phototoxicity against a Carcinoma Cell Line: A Computational and Experimental Study. *J. Chem.* **2017**, *2017*, 7365263.

(49) Oviedo, M. B.; Ilawe, N. V.; Wong, B. M. Polarizabilities of π-Conjugated Chains Revisited: Improved Results from Broken-Symmetry Range-Separated DFT and New CCSD(T) Benchmarks. *J. Chem. Theory Comput.h* **2016**, *12* (8), 3593−3602.

(50) Wong, B. M.; Hsieh, T. H. Optoelectronic and Excitonic Properties of Oligoacenes: Substantial Improvements from Range-Separated Time-Dependent Density Functional Theory. *J. Chem. Theory Comput.* **2010**, *6* (12), 3704−3712.

(51) Glembockyte, V.; Cosa, G. Redox-Based Photostabilizing Agents in Fluorescence Imaging: The Hidden Role of Intersystem Crossing in Geminate Radical Ion Pairs. *J. Am. Chem. Soc.* **2017**, *139* (37), 13227−13233.

(52) Tentscher, P. R.; Lee, M.; von Gunten, U. Micropollutant Oxidation Studied by Quantum Chemical Computations: Methodology and Applications to Thermodynamics, Kinetics, and Reaction Mechanisms. *Acc. Chem. Res.* **2019**, *52* (3), 605−614.